ACS OMEGA

http://pubs.acs.org/journal/acsodf

Article

Temperature-Limited Synthesis of Copper Manganites along the Borderline of the Amorphous/Crystalline State and Their Catalytic Activity in CO Oxidation

Hanna E. Solt, Péter Németh, Miklós Mohai, István E. Sajó, Szilvia Klébert, Fernanda Paiva Franguelli, Lara Alexandre Fogaca, Rajendra P. Pawar, and László Kótai*

Cite This: *ACS Omega* 2021, 6, 1523−1533

Read Online

ACCESS | Metrics & More | Article Recommendations | Supporting Information

ABSTRACT: Copper manganese oxides (CMO) with $CuMn_2O_4$ composition are well-known catalysts, which are widely used for the oxidative removal of dangerous chemicals, e.g., enhancing the CO to CO_2 conversion. Their catalytic activity is the highest, close to those of the pre-crystalline and amorphous states. Here we show an easy way to prepare a stable CMO material at the borderline of the amorphous and crystalline state (BAC-CMO) at low temperatures (<100 °C) followed annealing at 300 °C and point out its excellent catalytic activity in CO oxidation reactions. We demonstrate that the temperature-controlled decomposition of $[Cu(NH_3)_4](MnO_4)_2$ in $CHCl_3$ and CCl_4 at 61 and 77 °C, respectively, gives rise to the formation of amorphous CMO and NH_4NO_3, which greatly influences the composition as well as the Cu valence state of the annealed CMOs. Washing with water and annealing at 300 °C result in a BAC-CMO material, whereas the direct annealing of the as-prepared product at 300 °C gives rise to crystalline $CuMn_2O_4$ (sCMO, 15−40 nm) and ($(Cu,Mn)_2O_3$, bCMO, 35−40 nm) mixture. The annealing temperature influences both the quantity and crystallite size of sCMO and bCMO products. In 0.5% CO/0.5% O_2/He mixture the best CO to CO_2 conversion rates were achieved at 200 °C with the BAC-CMO sample (0.011 mol $CO_2/(m^2\ h)$) prepared in CCl_4. The activity of this BAC-CMO at 125 °C decreases to half of its original value within 3 h and this activity is almost unchanged during another 20 h. The BAC-CMO catalyst can be regenerated without any loss in its catalytic activity, which provides the possibility for its long-term industrial application.

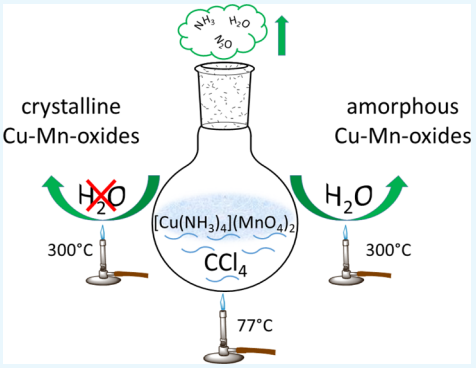

1. INTRODUCTION

Developing novel synthetic methods for catalytically active materials to improve their advantageous properties has attracted considerable interest. Copper manganese oxides (CMO) including spinel-type copper manganese oxides ($CuMn_2O_4$, sCMO) are important catalysts in the oxidative removal of harmful chemicals like organic volatiles such as toluene or formaldehyde,[1,23] hydrogen cyanide,[4] or nitric oxide.[5] They also show high CO to CO_2 conversion activity[6−8] including PROX (preferred oxidation of CO in CO−H_2 mixtures) reactions.[9] The catalytic performance strongly depends on their preparation methods, morphology, surface area, and crystallite size.[2,3,7,10−13] Furthermore, the application of various precursors, stoichiometry of the products, synthesis conditions, and ageing time profoundly influence the catalytic activity[6,11,14,15] mainly due to differences in the number and type of the redox couples at specific sites on the surface of the catalyst.[8,16] According to the literature data their activity is the highest in their amorphous state.[10,17,18] However, sCMOs lose their catalytic activity if the material is calcined at temperatures above ∼500 °C.[9,16] Thus, classical preparation routes of sCMO phases based on high temperature (>500 °C) solid-phase reactions of various precursors are less effective for synthesizing catalytically active materials.

A simple and easy way have been developed to prepare transition metal manganese oxides with 1:2 metal/Mn stoichiometry (e.g., spinel $CuMn_2O_4$) from the solid-phase redox reaction of the ammonia ligand and permanganate anion for a series of compounds $[M(NH_3)_4](MnO_4)_2$ (M = Cu, Zn, Cd). A key point of these syntheses is the application of liquid solvents as heat-absorbing media, which can control the decomposition temperature via the evaporation of solvent to absorb the reaction heat evolved.[19−23] Using $CHCl_3$ and CCl_4 as heat-absorbing media, the solid-phase redox reaction of $[Cu(NH_3)_4](MnO_4)_2$ can be performed at 61 and 77 °C, respectively. During the reaction $CuMn_2O_4$ and NH_4NO_3 are

Received: October 30, 2020
Accepted: December 22, 2020
Published: January 6, 2021

https://dx.doi.org/10.1021/acsomega.0c05301
ACS Omega 2021, 6, 1523−1533

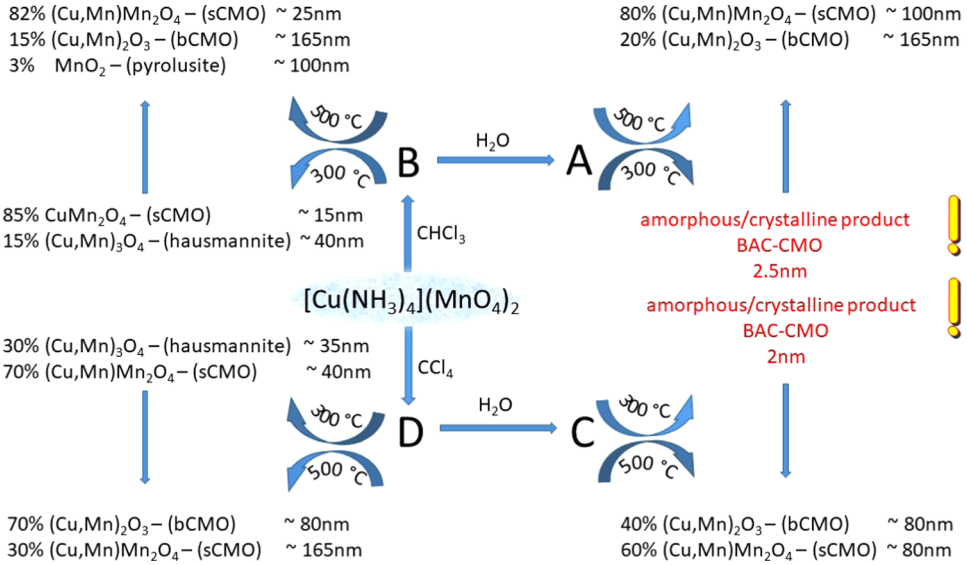

Figure 1. Decomposition of $[Cu(NH_3)_4](MnO_4)_2$ into copper manganese oxides in $CHCl_3$ (A, B) and CCl_4 (C,D) at 61 and 77 °C, respectively, with (A, C) and without (B, D) aqueous leaching.

formed, both of which are insoluble in chloroform and carbon tetrachloride.[19] NH_4NO_3 can be eliminated either by aqueous leaching (s = 208.9 g/100 g of water at 25 °C)[20,21] or thermal annealing.[19,22] Ammonium nitrate decomposes at around 200 °C in the CMO matrix with the formation of gaseous decomposition products (H_2O and N_2O) only.[19,22] To avoid wastewater formation, the thermal decomposition route was preferred previously to prepare the CMO samples.[19] The low temperature synthesis effectively inhibited crystal growth and resulted in the formation of amorphous materials, which are excellent candidates for enhancing the catalytic activity of CMOs.

Here we show an effective method for preparing CMOs rich in spinel-type ($CuMn_2O_4$, sCMO) and bixbyite-type ($(Cu,Mn)_2O_3$, bCMO) composites along the borderline of the amorphous and crystalline state (BAC-CMO) during low temperature (<100 °C) decomposition followed by annealing between 200 and 500 °C. We tune their catalytic properties via controlled composition, surface area, and crystallite size. We demonstrate that the formation of reactive ammonium nitrate as a co-decomposition product greatly influences the grain size, composition, and the Cu valence state of CMOs. We point out the effect of the recovery method (water washing and thermal decomposition), determine the phase relationship between sCMO and bCMO, and discuss their catalytic activity in the CO oxidation reaction.

2. RESULTS AND DISCUSSION

2.1. Preparation of Catalysts. [Tetraamminecopper(II) permanganate] was prepared and decomposed in $CHCl_3$ and CCl_4 under prolonged reflux according to the method developed by us.[22]

$$[Cu(NH_3)_4](MnO_4)_2 = CuMn_2O_4(\text{amorphous}) + 2NH_3 + NH_4NO_3 + H_2O \quad (1)$$

The key point of our preparation is that the reaction temperature cannot exceed the boiling point of the solvents (61 and 77 °C, in $CHCl_3$ and CCl_4, respectively), thus the syntheses are temperature-limited processes that could effectively inhibit nucleation and crystallization of the formed CMO samples driven by the exothermicity of decomposition reaction (289.8 kJ/mol).[22] In general, the CMO products can be characterized by the $CuMn_2O_{4+x}$ summarized formula, with x = 0 (sCMO, formally $CuMn_2O_4$) and x = 0.5 (bCMO, formally $CuMn_2O_{4.5}$ or $Cu_{0.67}Mn_{1.3}O_3$). These phases can "exchange" their cations, so the Cu/Mn ratios might vary in both phases. The summarized Cu/Mn ratio of the phases, however, must be equal to the Cu/Mn ratio (1:2) of $[Cu(NH_3)_4](MnO_4)_2$. The presence of Cu(I) or Mn(II) ions in sCMO and Cu(I, II) or Mn(II) ions in bCMO phases can give rise to crystalline defects and high valence Mn ions like Mn(IV).

In $CHCl_3$ at 61 °C (samples A and B) the decomposition was incomplete in 1 h. The water-washed sample A had a dark purple color and the X-ray diffraction (XRD) analysis (Supporting Information (SI) Figure 1) of sample B showed the presence of unreacted $[Cu(NH_3)_4(MnO_4)_2]$.

2.2. Effect of the Isolation Method on the Composition and Crystallinity of Catalysts. The water-washed, ammonium nitrate-free (A and C), and the unwashed NH_4NO_3 containing samples (B and D) were annealed between 200 and 500 °C for 1−8 h. The distribution of reaction products including their crystallite size are summarized in Figure 1.

Figure 1 shows that not only the reaction and annealing temperatures, but the method of NH_4NO_3 removal played a key role in the composition and crystallite size of the formed CMOs. To determine the optimal preparation conditions for the BAC-CMO samples having the best catalytic activity in CO oxidation (see below), we studied the influence of the annealing temperature and time in detail.

2.2.1. Properties of the Samples Prepared in $CHCl_3$. The amorphous CMO precursor formed in $CHCl_3$ (sample B) either transformed into a BAC-CMO product (grain size of 2.5 nm) or into nanocrystalline (grain size ~ 15 nm) sCMO and $(Cu,Mn)_3O_4$ (~40 nm) hausmannite mixture depending on whether the ammonium nitrate was washed out (former) or not (latter) before annealing at 300 °C. Further heating of the

https://dx.doi.org/10.1021/acsomega.0c05301
ACS Omega 2021, 6, 1523−1533

amorphous (sample A300-1h) and crystalline (sample B300-1h) products resulted in sCMO and bCMO with ~80:20 (A500-1h) (SI Figure 2) and ~80:15 (B500-1h) molar ratios, respectively. In sample B500-1h ~5% of MnO_2 pyrolusite could also be detected as a side product (Figure 2).

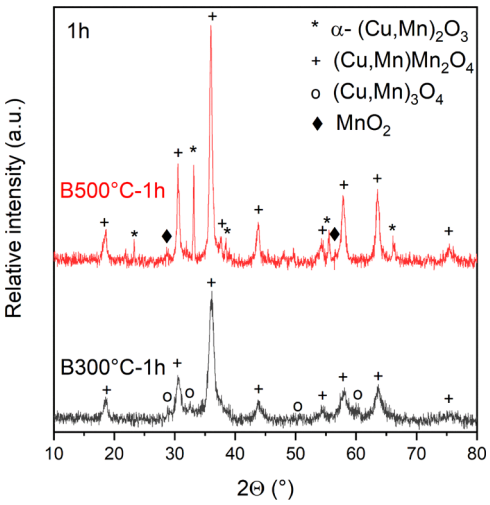

Figure 2. XRD of the samples prepared in $CHCl_3$ and annealed without washing (B) at 300 (black) and 500 °C (red).

Transformation of $(Cu,Mn)_3O_4$ hausmannite and Mn(II) in the B300-1h sample into bCMO and Mn(III) in the B500-1h sample was probably a result of a direct oxidation during heating to 500 °C by the oxygen content of the air.[23] Since NH_4NO_3 in sample B decomposed at around 200 °C, it does not play any direct role in the redox process. The decrease of the lattice constant from a = 0.8373 to 0.828 nm for the $(Cu,Mn)Mn_2O_4$ spinel (sCMO)[24] and that from a = 0.941 to 0.9352 nm for $(Cu,Mn)_2O_3$ bixbyite (bCMO) confirms the substitution of Mn(III) cations with copper(I,II) and manganese(II,IV) ions.

The crystallite sizes for the sCMO were ~100 and ~25 nm for the samples A500-1h and B500-1h (Figures 1 and 2 (SI)), respectively, whereas those of bCMO and MnO_2 pyrolusite in sample B500-1h were found to be ~165 and ~100 nm, respectively. The amount of sCMO in the sample prepared at 500 °C was much higher (~80%) than the amount of bCMO (~20%). The positive influence of ammonium nitrate on sCMO formation from metal nitrate precursors and the sCMO's activity in CO oxidation have been described.[23] We supposed that during heating molten NH_4NO_3 rise to a liquid film that could increase the mobility of ions and resulted in the formation of the sCMO product. However, the XRD investigation of sample A500-1h (washed with water before heating) showed that the sCMO:bCMO ratio was almost the same as in sample B500-1h, thus the accumulation of sCMO might not be attributed directly to the presence of NH_4NO_3. It is rather plausible that the solvent selection and the NH_4NO_3 isolation method (washing with water or thermal decomposition) had great influence on the NH_4NO_3 (see below). For completing the decomposition process in $CHCl_3$, the reaction time had to be increased up to 4 h. Due to higher decomposition temperature in CCl_4, the 1 h reaction time was proved to be enough to complete the decomposition of $[Cu(NH_3)_4](MnO_4)_2$, therefore we focused on the samples prepared in this solvent in our next experiments.

2.2.2. Properties of the Samples Prepared in CCl_4. The amorphous CMO precursor formed in CCl_4 after washing with water (C) or without washing with water (D) were annealed under the same conditions as samples (A) and (B). At 300 °C, BAC-CMO was formed from sample C with ~2 nm crystalline size, which transformed into a ~3:2 molar mixture of $(Cu,Mn)Mn_2O_4$ (a = 0.8373 nm, sCMO) and $(Cu,Mn)_2O_3$ (a = 0.941 nm, bCMO) with ~80−80 nm crystallite sizes at 500 °C (Figures 3 and 4 (SI)).

The presence of NH_4NO_3 in the starting amorphous material (D) resulted in the formation of a nanocrystalline $(Cu,Mn)Mn_2O_4$ spinel (~40 nm) and $(Cu,Mn)_3O_4$ hausmannite (~35 nm), respectively, in ~7:3 molar ratio at 300 °C. Further heating up to 500 °C induced oxidative decomposition of the Cu-substituted hausmannite and resulted in a $(Cu,Mn)Mn_2O_4$ spinel and $(Cu,Mn)_2O_3$ bixbyite mixture in ~3:7 molar ratio, with ~165 and ~80 nm crystallite size, respectively.

The presence or absence of ammonium nitrate in the starting samples D and C, respectively, substantially influenced the crystallinity and the composition (Figure 3).

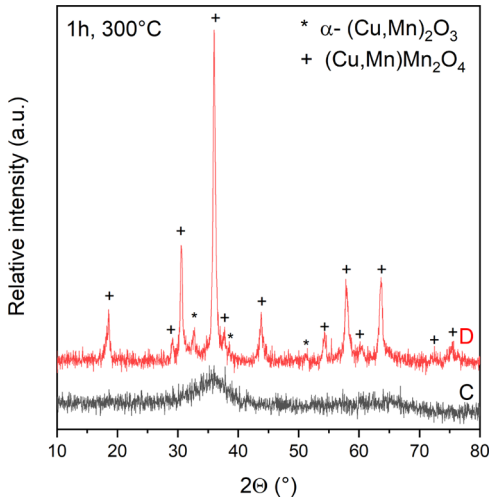

Figure 3. XRD of the samples prepared in CCl_4 and annealed with (C) and without washing (D) at 300 °C for 1 h.

Our experiments showed that the most promising catalyst in the CO oxidation was the BAC-CMO compound formed in CCl_4 after aqueous leaching (sample C) and annealing at 300 °C for 1 h. To optimize the reaction conditions to prepare this BAC-CMO catalyst species, the effect of annealing conditions were studied in detail (SI Figures 3−9). First of all, we investigated the composition of sample C, its starting material (sample D), and the proportion of the annealed sCMO and bCMO phases between 200 and 500 °C in air.

The results of N 1s X-ray photoelectron spectroscopy (XPS) studies on samples C, C300, and D300 unambiguously showed that the aqueous leaching could remove a large part of ammonium nitrate (N = 3.7 atom % in sample C) and annealing at 300 °C completed this process (C300) in 1 h. Similarly, the sample without washing also resulted in ammonium nitrate-free products (D300) by annealing at 300 °C for 1 h (SI Tables 1 and 2).

No hydrolysis/decomposition products of starting compound **1** ($Cu(OH)_2$, NH_4MnO_4)[24−26] were found in samples C and D because they decomposed on drying at 100 °C.[31]

https://dx.doi.org/10.1021/acsomega.0c05301
ACS Omega 2021, 6, 1523−1533

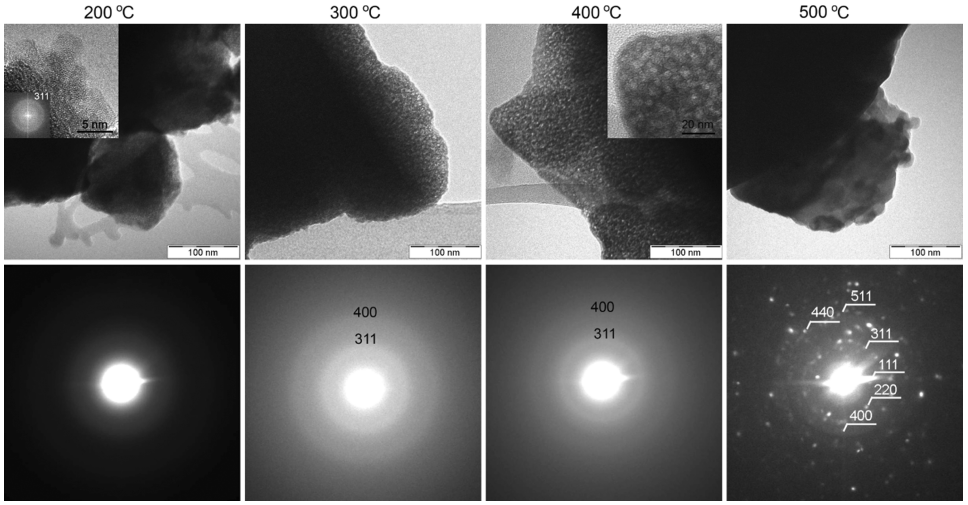

Figure 4. TEM images and diffraction patterns of sample C annealed between 200 and 500 °C.

Ammonium nitrate as the reaction product, however, could be detected with IR as ammonium and nitrate ions, and it could also be identified by XRD from the aqueous leachate (D → C) of sample D.[19,22] XRD analysis of sample D (SI Figure 1); however, did not show the presence of any crystalline form of ammonium nitrate.

To provide insights into the crystallization process we used transmission electron microscopy (TEM) to study the CMO samples annealed between 200 and 500 °C (Figure 4 and Table 1). Bright-field TEM images of samples annealed at 200

Table 1. Variation of Crystallite Sizes (Determined by the Scherrer Method) of Sample C (CCl_4, 1 h) under Annealing at 200−500 °C for 1 and 8 h

annealing			
temperature, °C	time, h	d(001) peak position of $CuMn_2O_4$,	average crystallite size, nm
200	1	~2.4	2
200	8	~2.5	2
300	1	~2.5	2
300	8	~2.5	2
400	1	~2.5	2
400	8	~2.5	2
500	1	2.544	80
500	8	2.544	80

°C showed 200 nm to 5 μm size grains that preserved the primary morphology of the precursor tetraamminecopper(II) permanganate. The electron diffraction (ED) patterns of the grains showed an amorphous halo indicating the lack of a long-range crystalline structure. The high-resolution TEM study of this material displayed the presence of subnanometer sized nanoclusters and their FFTs revealed a diffuse ring positioned at d ~ 0.25 nm spacing corresponding to the (311) plane of sCMO, which is the most dense crystallographic plane in the spinel structure. Therefore, we propose the material annealed at 200 °C has an amorphous structure, in which subnanometer size spinel clusters are present. As the annealing temperature increased, the cluster size became larger and larger and as a result the (311) reflection got sharper and sharper. In fact, the sample annealed at 300 °C showed ~ 2−5 nm size clusters and the (311) diffraction ring (as well as the (400)) was also evident on the ED pattern. TEM investigation showed practically no difference between the samples annealed at 300 and 400 °C. However, the sample formed at 500 °C was distinct having an ~50−100 nm average grain size of sCMO.

The presence of the finely dispersed NH_4NO_3 in the amorphous matrix might be attributed to the solid-phase quasi-intramolecular redox reaction, during which ammonia was locally oxidized into NH_4NO_3 at the lattice points of the former $[Cu(NH_3)_4](MnO_4)_2$, and simultaneously it induced the collapse of the crystal lattice without the re-arrangement of the residual ions into a new ordered crystalline structure.[19,20,22,27] The aqueous leaching of NH_4NO_3(D → C) did not result in obvious change in the XRD pattern of sample D (SI Figure 1). The presence of the finely dispersed ammonium nitrate, however, had a great influence on the crystallization behavior of amorphous CMO compounds during annealing. NH_4NO_3 melted at 169.6 °C and decomposed at ~ 200 °C in the CMO matrix, thus liquid NH_4NO_3 could initiate nucleation/crystal growth below 200 °C.[28]

Sample C was annealed stepwise between 400 and 500 °C for 1 h, and we found that the crystallization process completed above 460 °C. (SI Figure 5). Following this procedure, BAC-CMO phases can be prepared between 100 and 450 °C.

2.2.3. Surplus Oxygen Content in the Catalyst Samples. The quasi-intramolecular solid-phase reduction of permanganate are generally stepwise processes,[27] when the reduction of manganese(VII) and disproportionation of intermediate valence compounds (e.g., Mn(V), Mn(VI)) can result in the formation of manganese compounds having different valences. Typically, surplus oxygen content ($CuMn_2O_{4+x}$) can be attributed to the Mn(IV) content of the sCMO phases (x = $CuMn_2O_5/CuMn_2O_4$ molar ratio). This surplus oxygen content was determined by redox titrimetry reducing Mn(III) and higher Mn oxidation states into Mn(II) with oxalic acid. The titrimetry results for the samples of series C for 1−4 h annealing time between 200 and 500 °C are reported in Table 2.

The general tendency is that the average oxidation state of manganese is higher than III in all samples, and it is the highest in the starting sample C (x = 0.27). Supposing the regular Cu(II) and Mn(III) states in $CuMn_2O_{4+x}$, the surplus oxygen

https://dx.doi.org/10.1021/acsomega.0c05301
ACS Omega 2021, 6, 1523−1533

Table 2. Surplus Oxygen Content of $CuMn_2O_{4+x}$ Samples Prepared from Sample C (CCl_4, 80 °C, x = 0.27) by Annealing at 200−500 °C for 1−4 h

	temperature			
reaction time	200 °C	300 °C	400 °C	500 °C
1 h	0.19	0.19	0.14	0.11
2 h	0.17	0.18	0.15	0.11
3 h	0.16	0.19	0.15	0.12
4 h	0.14	0.19	0.15	0.10

content in sample C results in 9.0% tetravalent manganese content. The surplus oxygen content decreases gradually with increasing annealing temperature. Except at 200 °C, the annealing time has no substantial effect on the oxidation state of manganese, the thermal decomposition reaction is completed in the first hour of annealing. At 200 °C, however, the starting x = 0.27 value gradually decreases to almost half (x = 0.14) upon increasing the heating time to 4 h.

2.3. Valence Distribution of Metals in the Catalysts. The activity of the CMO catalyst depends on the presence of various mixed valence states of copper (Cu(I,II)) and manganese (Mn(II,III and IV)).[7,9,15] Thus, to elucidate the surface composition and chemical state of the metallic components on the surface of the fresh and used CMO samples XPS studies were performed. Figures 5−7 show the copper and manganese $2p_{3/2}$ XP spectra of some selected fresh and used catalyst samples, the C, O, and N 1s spectra are given in SI Figures 10−12. The results of the surface composition analysis calculated from the peak areas are given in SI Tables 1 and 2.

The decomposition of the Cu $2p_{3/2}$ signal reveals the valence states (0, I, or II) of the copper on the catalyst surface (SI Table 1). The available information about the positions of Cu(I) and Cu(II) signals in the XPS spectra of cubic spinel, particular amorphous, are controversial.[29−31] The intensity changes of the shake-up peaks of Cu(II) (~942 eV) correlate well with those occurring at 934.5 and 932.9 eV, thus we presume that all of these peaks belong to Cu(II) ions only and not to Cu(I) or Cu(0) signals (Figures 5 and 13 (SI)). Therefore, for samples C300, C300 used, D300, and D500, we assign the XPS peaks at 932.9 and 934.5 to octahedrally- and tetrahedrally-coordinated Cu(II), respectively, whereas the peaks at 930.8 could belong to either the Cu(0) or Cu(I) signal.[29,30] The kinetic energy of the Auger $Cu_{LV\,V}$ region, can be used to distinguish metallic and Cu(I) surface species. Based on this distinction, metallic copper does not appear in our samples. The Cu 2p signals of Cu(I) for our sCMO phases indicates the existence of Cu(I) only in the tetrahedral position (930.6 eV), because no peaks appear below 930 eV, which would indicate octahedrally-coordinated Cu(I).[32] Also the ~935 eV[31] peak is missing, which suggests the lack of copper carbonates in the sample used in CO oxidation (C300-1h-used) (Figure 6).

The deconvolution of the Mn $2p_{3/2}$ signal is useful for distinguishing among the states of Mn(II), Mn(III), and Mn(IV) (SI Table 1).[9] The peaks located at ~640.8, 642.4, and 644.3 eV can be associated with Mn(II), Mn(III), and Mn(IV), respectively.[33]

Since the Cu(II)/Cu(I) ratio has an influence on the surface Cu:Mn ratio, $ZnMn_2O_4$ was also studied because Zn can only be divalent. Decomposition of $[Zn(NH_3)_4](MnO_4)_2$ in toluene resulted in $ZnMn_2O_4$ with a 0.27 nm thick ZnO surface layer (Mn/Zn becomes ~1:1).[34] Thus, the deficiency of Mn in the surface layer of CMO samples was attributed to the formation of a surface oxide layer (Cu_xO, x = 1 or 2).[33,35] Thus, we infer that the surface layers of CMO samples are richer in oxygen than the analogous $ZnMn_2O_4$ (Table 3). The O/Cu values for the CMO type sample D are higher than those for CMO samples C, presumably due to copper defects, presence of hydroxyl groups, or high valence Mn-species on the surface of samples D. Our XPS study, however, does not indicate any substantial difference in the Mn(IV) content on the surface region of C or D sample series. The phase relations of D type CMOs differ from that of sample C type CMOs.[36−39]

This difference might play a key role in the activity of the samples, we assume the higher sCMO content and the smaller size (borderline state) might be responsible for the higher catalytic activity of sample C in CO oxidation than that of samples D annealed under identical conditions.

Since Cu(I) and Mn(II) preferentially occur in tetrahedral sites, while Cu(II), Mn(III), and Mn(IV) are dominantly located in the octahedral sites of the spinel lattice, the following general formula for the CMO phases can be generated: $(Cu_x^{I}Mn_{1-x}^{II})_T\ (Cu_{1-x}^{II}\ Mn_x^{IV}\ Mn^{III})_OO_4$ where T and O denotes the tetrahedral and octahedral positions,[29] respectively. Our results, however, indicate a rather complicated formula due to the presence of large number of defects arising from pre-crystalline, amorphous, and the multiphase nature of the annealed products. The peak intensities of Cu(II) and Cu(I) signals in the XP spectra of sample C, C300-1h and used C300-1h are very similar, we presume that Cu(I)/Cu(II) concentrations in the surface layers did not change on heating of sample C up to 300 °C for 1 h, or during five catalytic cycles (Figure 8). The level of Cu(I) is low, ~1 atomic %. The amount of surface Mn(II) and Mn(IV) increases and Mn(III) decreases on heating sample C up to 300 °C for 1 h.

The decrease of surface Mn(III) and Mn(IV) concentrations and the increase of Mn(II) concentration of the used C300-1h

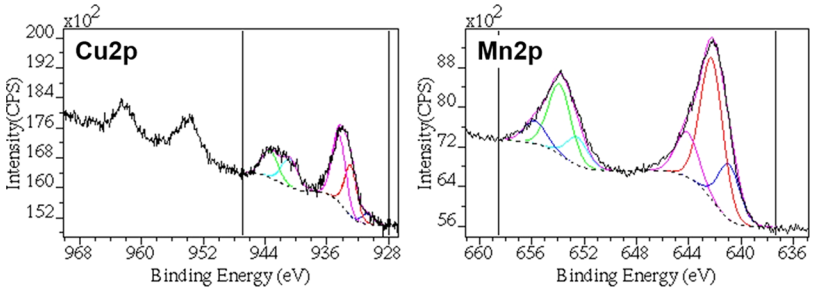

Figure 5. Cu 2p and Mn 2p XPS spectra of sample C (CCl_4, 2 h) without annealing.

https://dx.doi.org/10.1021/acsomega.0c05301
ACS Omega 2021, 6, 1523−1533

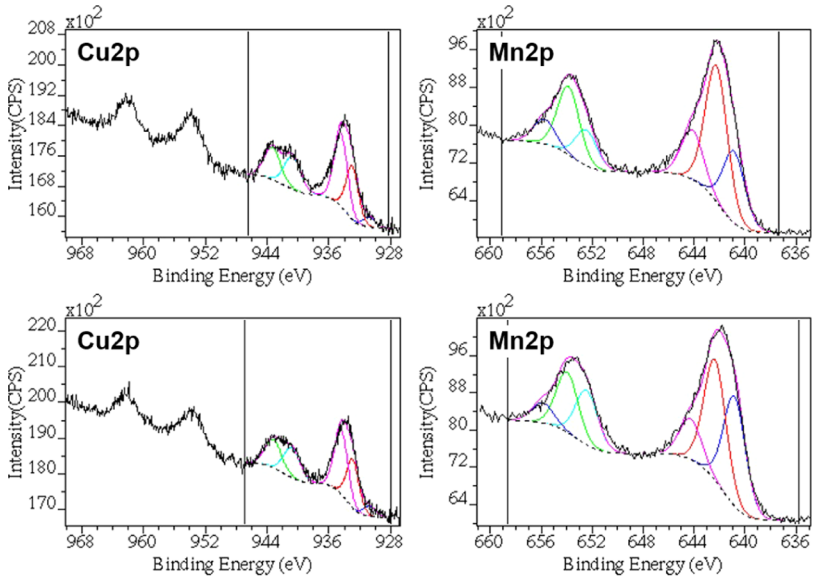

Figure 6. Cu 2p and Mn 2p XPS spectra of fresh (top) and used (5 cycle in CO oxidation, 125 °C, >20 h) (bottom) sample C (CCl_4, 2 h) annealed at 300 °C for 1 h.

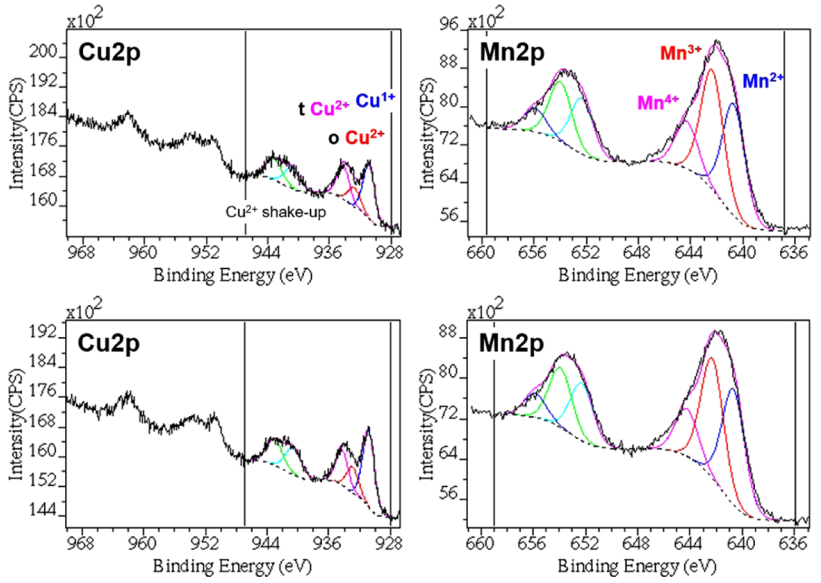

Figure 7. Cu 2p and Mn 2p XPS spectra of sample D (CCl_4, 2 h, without washing) annealed at 300 (top) and 500 °C (bottom) for 1 h.

Table 3. Surface Atomic Ratios of Main Constituents Calculated Using Various Photoelectron Lines Applying the Multiline Approach of Hanke et al.[33]

sample	lines	Mn/Cu Mn/Zn	O/Cu O/Zn
$ZnMn_2O_4$	Zn $2p_{3/2}$, Mn 2p	1.07	3.81
	Zn $2p_{3/2}$, Zn 3p, Mn $2p_{3/2}$, Mn $2p_{1/2}$, Mn 3p	1.10	3.81
	Zn $2p_{3/2}$,Mn $2p_{1/2}$	1.01	3.79
	Zn 3p, Mn $2p3_{/2}$	1.10	3.82
	Zn 3p, Mn 3p	1.09	3.80
Sample C	Cu $2p_{3/2}$, Mn 2p	1.37	4.24
C300-1h	Cu $2p_{3/2}$, Mn 2p	1.42	3.90
C300-1h-used	Cu $2p_{3/2}$, Mn 2p	1.56	4.23
D300-1h	Cu $2p_{3/2}$, Mn 2p	2.21	5.69*
D500-1h	Cu $2p_{3/2}$, Mn 2p	1.87	5.05*

sample in comparison to corresponding concentrations obtained for fresh C300-1h can be attributed to the reduction of Mn(IV) and Mn(III) during CO oxidation and simultaneous Mn(II) formation.

We investigated the influence of ammonium nitrate for the valence distributions of metals by comparing the XPS spectra of C300-1h and D300-1h samples. We found the amount of Cu(I) and Mn(II) were much higher in sample D300-1h than in sample C300-1h (Figure 8). The Mn(IV) level were practically identical in both samples but the surface Mn(III) content was reduced for the D300-1 samples as a result of molten ammonium nitrate induced reduction process.

A key point of the XPS study is the lack of a preferential site for Cu(II) reduction, which is evidenced by the proportional change of Cu(II) concentrations in the tetrahedral and octahedral positions. (Figure 8).

https://dx.doi.org/10.1021/acsomega.0c05301
ACS Omega 2021, 6, 1523−1533

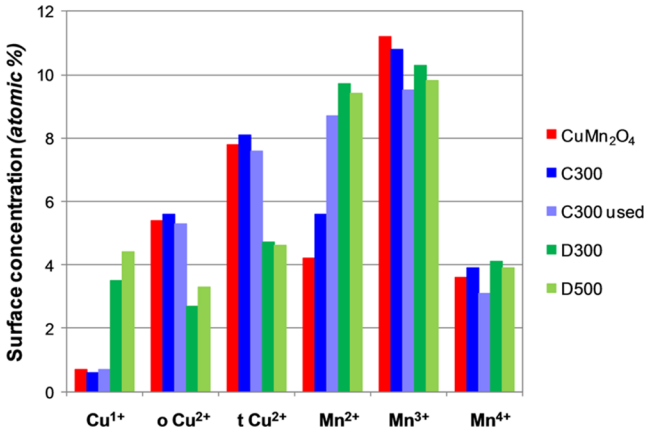

Figure 8. Surface concentrations of Cu(I,II) and Mn(II–IV) species on the catalyst samples prepared in CCl_4 at 77 °C with various post-treatment.

The temperature dependence of valence distributions were tested in samples D300-1h and D500-1h. The Cu(I) concentrations increases with increasing temperature, whereas the Cu(II) level at the tetrahedral sites slightly decreases. Since ammonium nitrate decomposes below 300 °C, the increase of the Cu(I)/Cu(II) concentrations might be the consequence of the redox reactions induced by the manganese species only. As a result of decreasing Mn(II) and Mn(III) concentrations, the reduction of tetrahedrally-coordinated Cu(II) to Cu(I) increases. The oxidation of Mn(II) ions might be attributed to the Cu(II) + Mn(II) = Cu(I) + Mn(III) reaction, but it can also be driven by the oxidation of Mn(III) into Mn(IV) in air. The oxidation is confirmed with the increasing O/Mn ratio (from 2.69 to 2.81 in D300-1h and D500-1h samples, respectively), and suggests that the surface oxygen surplus is associated with the manganese content (Figure 8). The high Cu(I) concentration predestines that the samples of series D could become a good catalyst for CO oxidation; however, the samples of series C were found to be definitely more active catalysts (see below) than the samples from series D.

Our XPS study demonstrates that the preparation method greatly influences the phase and chemical composition of CMO catalyst precursors, thus the catalytic behavior is expected to vary even for samples prepared with similar composition but via different reaction routes.

2.4. Surface Areas of CMO Samples. The surface areas were found to be low enough in all series of samples even in those used in the catalytic cycle (Table 4 and Figure 9). The total pore volume of sample C was found to be ~0.14 cm^3/g at a 58 m^2/g specific surface area, the diameter of micropores and mesopores were determined to be 1.5 and 11 nm, respectively, the amount of cumulative micropores and mesopores were found to be ~0.02 and 0.14 cm^3/g, respectively.

Table 4. Surface Area of bCMO and sCMO-Rich Samples Prepared at Various Temperatures

sample	surface area, m^2/g
C	58
A300-1h	29.7 (29.4)[a]
C300-1h	4.6
C300-8h	6.8
C500-1h	14.2
C500-8h	10.9[a]
D300-1h	24[a]
D500-1h	11.1[a]

[a]Used catalyst in a catalytic cycle.

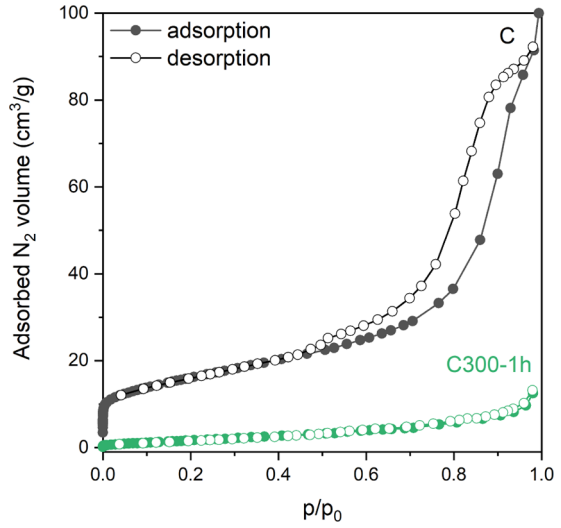

Figure 9. N_2 adsorption–desorption isotherms of sample C (amorphous CMO).

According to the classification of isotherms by IUPAC, the nitrogen adsorption/desorption isotherm of sample C is type IV with the characteristic hysteresis loops of H4, which is usually associated with activated carbons or other adsorbent with slit-shaped pores. The surface area decreases with increasing annealing temperature.

2.5. Catalytic Oxidation of CO in the Presence of CMO Catalysts. The activity of sCMO-rich, bCMO-rich, and BAC-CMO catalysts were tested in the oxidative conversion of CO in 0.5% CO/0.5% O_2/He mixture between room temperature and 200 °C. The effect of preparation conditions on the activity of samples annealed at 300 °C are given in Figure 10.

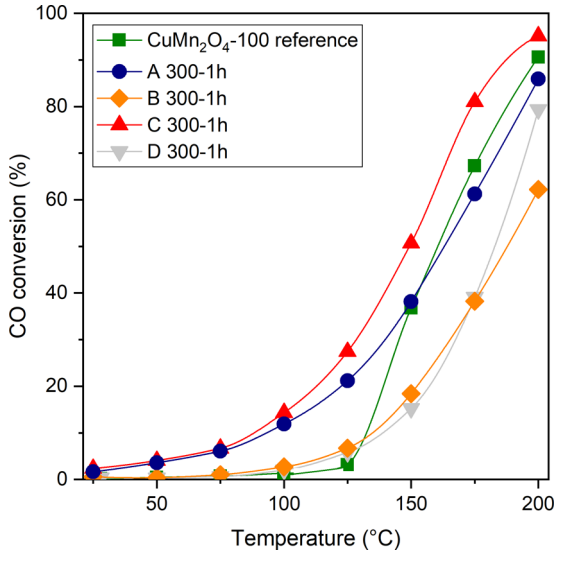

Figure 10. Comparison of CO oxidation by the samples annealed at 300 °C and prepared in various ways (A–D). Reactant flow: 0.5% CO, 0.5% O_2/He; 1.37 $g_{CO} \times g_{cat}^{-1} \times h^{-1}$.

https://dx.doi.org/10.1021/acsomega.0c05301
ACS Omega 2021, 6, 1523–1533

The highest catalytic activity among the samples annealed at 300 °C was found for the C300-1h (~95%) and the A300-1h (~80%) products. Therefore, we presume that the washing out of NH_4NO_3 and using CCl_4 at higher temperature (77 °C) than $CHCl_3$ (61 °C) have advantageous effects on the catalytic activity of bCMO/sCMO samples in CO oxidation. There were no deactivation of samples C300-1h and D300-1h, whereas the samples prepared in chloroform showed remarkable deactivation (SI Figure 14), thus we performed the catalytic activity studies for the samples prepared in CCl_4 and in particular for the series of samples C (Figure 11).

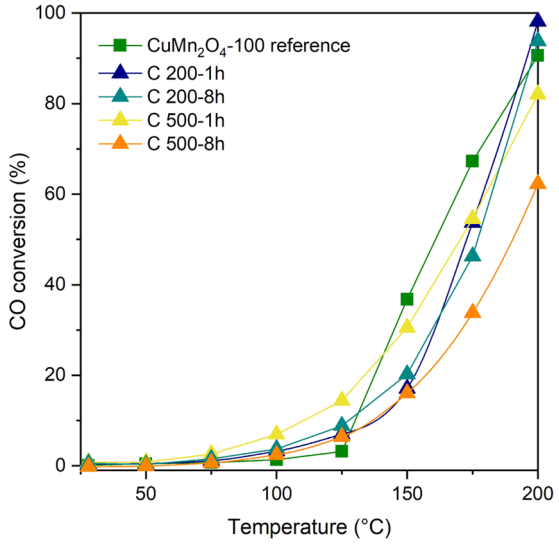

Figure 11. Effect of annealing temperature and time on the activity of sample C (CCl_4, aqueous leaching) on the catalytic activity in CO oxidation between 25 and 200 °C. Reactant flow: 0.5% CO, 0.5% O_2/He; 1.37 $g_{CO} \times g_{cat}^{-1} \times h^{-1}$.

The effect of annealing temperature of the catalysts prepared between 200 and 500 °C were studied on their catalytic activity in the CO oxidation reaction in detail (Table 5). The

Table 5. Temperature Dependence of the Catalytic Activity (10, 25, and 50% CO Conversion Temperatures) of CMO Samples in CO Oxidation

catalyst	T_{10}, °C	T_{25}, °C	T_{50}, °C
C	121	130	161
A300-1h	94	132	163
B300-1h	134	159	188
C300-1h	88	121	149
D300-1h	138	162	183
C200-1h	135	155	173
C200-8h	127	155	177
C500-1h	111	142	170
C500-8h	137	164	190
D500-1h	166	190	>200

results showed that the increase of the annealing temperature decreased the catalytic activity in CO oxidation. The most active samples (C type) were also investigated to understand the effect of annealing time on the catalytic activity of samples prepared between 200 and 500 °C (Figure 10). The samples annealed between 200 and 500 °C for 1 h were proved to be catalytically more active in the CO oxidation than the samples annealed at the same temperatures for a longer time (8 h). The catalytic activities of sample C in the CO oxidation reaction annealed at 200 and 300 °C for 1−1 h, respectively, were practically the same (98 and 95%), but the activity of C200-1h was proved to be less than that of C300-1h at lower temperatures (10 and 50% or 50 and 80% conversions at 150 or 175 °C, respectively).

We tested the catalytic performance of sample C300-1h (BAC-CMO) during 5 cycles and long (22−25 h) measurements (SI Figure 15). The results showed that at 125 °C the catalytic activity decreased with increasing reaction time from 5×10^{-3} to 2.5×10^{-3} mol $CO_2/(m^2\ h)$. The decrease was particularly rapid in the first three hours. Such kind of activity profile is characteristic of the commercial hopcalite-type CO oxidation catalysts.[12] The results indicated that the sample C300-1h (BAC-CMO) could be recycled without changing its activity profile. The BAC-CMO catalyst becomes stable after the 1st cycle and its activity does not change in the next four cycles.

In summary we found an easy way to prepare amorphous CMO samples, which can be used as catalysts in CO oxidation and have comparable stability and activity as the commercial hopcalyte-type catalysts.

3. CONCLUSIONS

Thermal decomposition of tetraamminecopper(II) permanganate under temperature-controlled conditions (in $CHCl_3$ and CCl_4 at 61 and 77 °C, respectively) resulted in the formation of amorphous CMO and ammonium nitrate mixture. Ammonium nitrate removal with aqueous washing and annealing at 300 °C gave rise to BAC-CMO with excellent catalytic activity in the oxidation reaction of carbon monoxide. At 500 °C the BAC-CMO samples transformed to ~8:2 (~100 and ~165 nm) and ~6:4 ratio (80 and 80 nm) sCMO and bCMO products, respectively. We found that the applied solvent ($CHCl_3$ or CCl_4) and the annealing temperature (300 or 500 °C) influenced the composition and crystallite sizes of sCMO and bCMO. The bCMO content was higher in samples prepared in CCl_4 than those prepared in $CHCl_3$ under analogous annealing conditions. The catalytic activity of the amorphous samples in CO oxidation was high (0.5% CO, 0.5% O_2 in He,~200 °C), we obtained the best results with the samples prepared in CCl_4 and annealed at < 300 °C (0.011 mol CO/m^2 catalyst/h). Higher annealing temperature decreased the catalytic activity. The experiment with the long-term catalyst (CCl_4, 300 °C, 1 h) showed decreasing activity similar to commercial hopcalite. It is intriguing that the catalysts could be regenerated without loss of activity, which draws attention to its possible industrial application.

4. EXPERIMENTAL SECTION

All of the chemicals used (copper(II) sulfate pentahydrate, 25% aqueous ammonia, sulfuric acid, ammonium acetate), and the analytical reagents (oxalic acid, potassium permanganate, 8-hydroxyquinoline) and solvents (methanol, acetic acid, bidistilled water) were supplied by Deuton-X Ltd, (the correct name is : Deuton-X Ltd) Hungary.

[Tetraamminecopper(II)] permanganate was prepared from [tetraamminecopper(II)] sulfate monohydrate (2.0 g) dissolved in a mixture of 10 mL of water and 10 mL of ammonia solution (25%). The mixture was cooled to +5 °C, then 70 mL of $KMnO_4$ solution (46 g/L) was added and it was cooled back

https://dx.doi.org/10.1021/acsomega.0c05301
ACS Omega 2021, 6, 1523−1533

to +7 °C. The combined mixture was cooled to +2 °C in 8 min and it was left to stand for another 3 min. Finally, the combined mixture was filtered rapidly (G2 glass filter, water pump vacuum) and the product was dried in a desiccator at +2 °C. Dry [tetraamminecopper(II)] permanganate (1.4 g) was suspended in an appropriate solvent ($CHCl_3$ or CCl_4) and the combined mixture was heated until boiling of the solvent in a reflux condenser with intensive stirring. The mixtures were refluxed for 1 h. The brownish-black precipitates (CMO + NH_4NO_3) were filtered off (G4 glass filter, vacuum) and dried at room temperature. The following procedures were applied to the filtered materials:

- Sample A—decomposition in boiling $CHCl_3$ and washing with water.
- Sample B—decomposition in boiling $CHCl_3$ without washing with water.
- Sample C—decomposition in boiling CCl_4 and washing with water.
- Sample D—decomposition in boiling CCl_4 without washing with water.

We used 3 × 20 mL of water to remove all NH_4NO_3. The water-washed (A and C) and unwashed (B and D) samples were dried in air at 100 °C for 1 h and were called to be "dried" samples. These dried samples were annealed at 200, 300, 400 and 500 °C for 1, 2, 4 and 8 h in air. Sample (C) was also annealed in air atmosphere between 400 and 480 °C with 10 °C steps.

4.1. Catalyst Characterization. The active oxygen content of each sample was determined by the addition of oxalic acid and 20% aqueous sulfuric acid under prolonged boiling (30−60 min) until complete dissolution of the sample, and then the excess oxalic acid content was measured by titrimetry with 0.05 M potassium permanganate solution. The metal-content (Cu and Mn) was determined by gravimetry as 8-oxyquinolinate or inductively coupled plasma (ICP) measurement following the standard procedure.[22,23]

X-Ray diffraction analysis was performed on an Enraf Nonius FRS90 X-ray generator with a Cu Kα source fitted with an INEL CPS 1201 position sensitive detector.

Surface area analysis was conducted by N_2 adsorption at −196 °C using a volumetric computer-controlled surface analyzer AUTOSORB-1C (producer: Quantachrome). The Brunauer−Emmett−Teller (BET) surface area was calculated using the Brunauer−Emmett−Teller model. All samples were degassed in vacuum for 24 h at 100 °C prior to analysis.

Transmission electron microscopy investigations were performed on a Morgagni 268D operating at 100 kV accelerating voltage and a JEOL 2010 electron microscope operating at 200 kV. We applied bright-field imaging and electron diffraction for morphological and phase analysis, respectively. Fast Fourier transform was calculated using Gatan Digital Micrograph 3.6.1 software.

For catalytic experiments of CO oxidation, 25 mg of catalysts with a grain size of 0.25−0.50 mm were placed in a U-shape flow-through microreactor (I.D. 4 mm) between two quartz wool plugs and pre-treated in a 30 cm^3/min helium flow at 200 °C for 1 h. The heating rate was 10 °C/min. After cooling to 25 °C in a helium flow, 100 cm^3/min reactant mixture containing 0.5% CO and 0.5% O_2 in remaining helium (1.37 $g_{CO} \times g_{cat}^{-1} \times h^{-1}$) was led through the catalyst bed. The reaction temperature was increased from 25 to 200 °C in 25 °C increments. The effluent gas composition was analyzed using an online mass spectrometer (VG ProLab, Thermo Scientific) following mass numbers (m/z) 4, 28, 32, and 44. The CO conversion at each reaction temperature was determined after 20−30 min time on stream.

X-ray photoelectron spectra were recorded on a Kratos XSAM 800 spectrometer operated in the fixed analyzer transmission mode with 40 eV pass energy, using Mg $K\alpha_{1,2}$(1253.6 eV) excitation. The pressure of the analysis chamber was lower than 1×10^{-7} Pa. Survey spectra were recorded for all samples in the 100−1300 eV kinetic energy range with 0.5 eV steps and 0.5 s dwell time. High-resolution spectra of the characteristic photoelectron lines of the main constituent elements, Cu 2p, Mn 2p, O 1s, and C 1s contaminations, were recorded by 0.1 eV steps and 1 s dwell time. Decomposition of the Cu 2p and Mn 2p spectra to various chemical states was based on the works of Fortunato et al.[37] and Valdés-Solís et al.[9] The spectra were referenced to the binding energy of the components of the Cu 2p and Mn 2p lines. Quantitative analysis, based on peak area intensities (after removal of the Shirley type background), was performed using the XPS MultiQuant[35] program using experimentally determined photo-ionization cross-section data of Evans[38] and asymmetry parameters of Reilman.[39]

■ ASSOCIATED CONTENT

Supporting Information

The Supporting Information is available free of charge at https://pubs.acs.org/doi/10.1021/acsomega.0c05301.

Powder XRD of copper manganese oxides prepared under various conditions; O 1s, N 1s, and C 1s XP spectra; shape and intensity of Cu(II) shake-up bands compared with the intensity changes of Cu(I) signals; carbon monoxide conversion in the 25−200 °C temperature range; CO conversion at 125 °C as a function of the time on stream; XPS binding energy and chemical state assignment of metallic components; O 1s, N 1s, C 1s, Cu 2p, and Mn 2p XPS results; N_2 isotherm data (PDF)

■ AUTHOR INFORMATION

Corresponding Author

László Kótai − *Institute of Materials and Environmental Chemistry, Research Centre for Natural Sciences, Budapest H-1117, Hungary; Deuton-X Ltd., Érd 2030, Hungary;* orcid.org/0000-0001-6375-3120; Email: kotai.laszlo@ttk.mta.hu

Authors

Hanna E. Solt − *Institute of Materials and Environmental Chemistry, Research Centre for Natural Sciences, Budapest H-1117, Hungary;* orcid.org/0000-0002-9888-2894

Péter Németh − *Institute of Materials and Environmental Chemistry, Research Centre for Natural Sciences, Budapest H-1117, Hungary; Department of Earth and Environmental Sciences, University of Pannonia, Veszprém H-8200, Hungary;* orcid.org/0000-0001-5592-5877

Miklós Mohai − *Institute of Materials and Environmental Chemistry, Research Centre for Natural Sciences, Budapest H-1117, Hungary;* orcid.org/0000-0002-5162-1590

István E. Sajó − *Szentágothai Research Center, University of Pécs, Pécs H-7624, Hungary*

https://dx.doi.org/10.1021/acsomega.0c05301
ACS Omega 2021, 6, 1523−1533

Szilvia Klébert − *Institute of Materials and Environmental Chemistry, Research Centre for Natural Sciences, Budapest H-1117, Hungary;* orcid.org/0000-0002-3107-3371
Fernanda Paiva Franguelli − *Institute of Materials and Environmental Chemistry, Research Centre for Natural Sciences, Budapest H-1117, Hungary; Department of Inorganic and Analytical Chemistry, Budapest University of Technology and Economics, Budapest H-1111, Magyarország*
Lara Alexandre Fogaca − *Institute of Materials and Environmental Chemistry, Research Centre for Natural Sciences, Budapest H-1117, Hungary; Department of Inorganic and Analytical Chemistry, Budapest University of Technology and Economics, Budapest H-1111, Magyarország*
Rajendra P. Pawar − *Organic Chemistry Department, Deogiri College, Aurangabad 431005, Maharastra, India*

Complete contact information is available at: https://pubs.acs.org/10.1021/acsomega.0c05301

Notes

The authors declare no competing financial interest.

■ ACKNOWLEDGMENTS

The research within project No. VEKOP-2.3.2-16-2017-00013 was supported by the European Union and the State of Hungary, co-financed by the European Regional Development Fund. P.N. acknowledges financial support from GINOP-2.3.2-15-2016-00053, János Bolyai Research Scholarship, and the ÚNKP-20-5-PE-7 New National Excellence program of the ministry for innovation and technology.

■ REFERENCES

(1) Kamal, M. S.; Razzak, S. A.; Hossain, M. M. Catalytic oxidation of volatile organic compounds (VOCs) − A review. *Atmos. Environ.* **2016**, *140*, 117−134.
(2) Ye, Z.; Giraudon, J. M.; Nuns, N.; Simon, P.; Geyter, N. D.; Morent, R.; Lamonier, J. F. Influence of the preparation method on the activity of copper-manganese oxides for toluene total oxidation. *Appl. Catal., B* **2018**, *223*, 154−166.
(3) Liu, P.; Wei, G.; Liang, X.; Chen, D.; He, H.; Chen, T.; Xi, Y.; Chen, H.; Han, D.; Zhu, J. Synergetic effect of Cu and Mn oxides supported on palygorskite for the catalytic oxidation of formaldehyde: Dispersion, microstructure, and catalytic performance. *Appl. Clay Sci.* **2018**, *161*, 265−273.
(4) Li, Y.; Yang, H.; Zhang, Y.; Hu, J.; Huang, J.; Ning, P.; Tian, S. Catalytic decomposition of HCN on copper manganese oxide at low temperatures: Performance and mechanism. *Chem. Eng. J.* **2018**, *346*, 621−629.
(5) Shi, C.; Chang, H.; Wang, C.; Zhang, T.; Peng, Y.; Li, M.; Wang, Y.; Li, J. Improved Activity and H_2O Resistance of Cu-Modified MnO_2 Catalysts for NO Oxidation. *Ind. Eng. Chem. Res.* **2018**, *57*, 920−926.
(6) Hutchings, G. J.; Mirzaei, A. A.; Joyner, R. W.; Siddiqui, M. R. H.; Taylor, S. H. Effect of preparation conditions on the catalytic performance of copper manganese oxide catalysts for CO oxidation. *Appl. Catal., A* **1998**, *166*, 143−152.
(7) Krämer, M.; Schmidt, T.; Stöwe, K.; Maier, W. F. Structural and catalytic aspects of sol−gel derived copper manganese oxides as low-temperature CO oxidation catalyst. *Appl. Catal., A* **2006**, *302*, 257−263.
(8) Schwab, G. M.; Kanungo, S. B. Die katalytische Verstärkung im Hopcalit. *Z. Phys. Chem.* **1977**, *107*, 109−120.
(9) Valdés-Solís, T.; Lopez, I.; Marban, G. Copper manganite as a catalyst for the PROX reaction. Deactivation studies. *Int. J. Hydrogen Energy* **2010**, *35*, 1879−1887.
(10) Rangappa, D.; Ohara, S.; Umetsu, M.; Naka, T.; Adschiri, T. Synthesis, characterization and organic modification of copper manganese oxide nanocrystals under supercritical water. *J. Supercrit. Fluids* **2008**, *44*, 441−445.
(11) Zhao, H.; Zhou, X.; Huang, W.; Pan, L.; Wang, M.; Li, Q.; Shi, J.; Chen, H. Effect of Potassium Nitrate Modification on the Performance of Copper-Manganese Oxide Catalyst for Enhanced Soot Combustion. *ChemCatChem* **2018**, *10*, 1455−1463.
(12) Tang, Z.-R.; Jones, C.; Aldridge, J. W.; Davies, T.; Bartley, J.; Carley, A.; Taylor, S.; Allix, M.; Dickinson, C.; Rosseinsky, M.; Claridge, J.; Xu, Z.; Crudace, M.; Hutchings, G. New Nanocrystalline Cu/MnOx Catalysts Prepared from Supercritical Antisolvent Precipitation. *ChemCatChem* **2009**, *1*, 247−251.
(13) Tang, Z. R.; Kondrat, S. A.; Dickinson, C.; Bartley, J. K.; Carley, A. F.; Taylor, S. H.; Davies, T. E.; Allix, M.; Rosseinsky, M. J.; Claridge, J. B.; Xu, Z.; Romani, S.; Crudace, M. J.; Hutchings, G. J. Synthesis of high surface area $CuMn_2O_4$ by supercritical anti-solvent precipitation for the oxidation of CO at ambient temperature. *Catal. Sci. Technol.* **2011**, *1*, 740−746.
(14) Mirzaei, A. A.; Shaterian, H. R.; Habibi, M.; Hutchings, G. J.; Taylor, S. H. Characterisation of copper-manganese oxide catalysts: effect of precipitate ageing upon the structure and morphology of precursors and catalysts. *Appl. Catal., A* **2003**, *253*, 499−508.
(15) Buciuman, F. C.; Patcas, F.; Hahn, T. Synergy effect between copper and manganese oxides in hopcalite catalysts. *Stud. Surf. Sci. Catal.* **2001**, *138*, 315−322.
(16) Vepreck, S.; Cocke, D. L.; Kehl, S.; Oswald, H. R. Mechanism of the deactivation of Hopcalite catalysts studied by XPS, ISS, and other techniques. *J. Catal.* **1986**, *100*, 250.
(17) Wright, P. A.; Natarajan, S.; Thomas, J. M.; Gai-Boyes, P. L. Mixed-Metal Amorphous and Spinel Phase Oxidation Catalysts: Characterization by X-ray Diffraction, X-ray Absorption, Electron Microscopy, and Catalytic Studies of Systems Containing Copper, Cobalt, and Manganese. *Chem. Mater.* **1992**, *4*, 1053−1065.
(18) Deraz, N. M.; Abd-Elkader, O. H. Synthesis and Characterization of Nano-crystalline Bixbyite-Hopcalite Solids. *Int. J. Electrochem. Sci.* **2013**, 10112−10120.
(19) Kotai, L.; Nemeth, P.; Kocsis, T.; Sajo, I. E.; Pasinszki, T.; Szilagyi, M. A.; Kant, R.; Pawar, R. P.; Sharma, P. K. A new route to synthesize controlled-size MMn_2O_4-type transition metal (M=Cd, Zn, Cu) nanomanganites. *Nano Studies* **2016**, *13*, 7−13.
(20) Sajó, I. E.; Kotai, L.; Keresztury, G.; Gacs, I.; Pokol, G. Y.; Kristóf, J.; Soptrayanov, B.; Petrusevski, V. M.; Timpu, D.; Sharma, P. K. Studies on the Chemistry of Tetraamminezinc(II) Dipermanganate ($[Zn(NH_3)_4](MnO_4)_2$): Low- Temperature Synthesis of the Manganese Zinc Oxide ($ZnMn_2O_4$) Catalyst Precursor. *Helv. Chim. Acta* **2008**, *91*, 1646−1658.
(21) Kótai, L.; Sajó, I. E.; Jakab, E.; Keresztury, G.; Németh, C.; Gács, I.; Menyhárd, A.; Kristóf, J.; Hajba, L.; Petrusevski, V. M.; Ivanovski, V.; Timpu, D.; Sharma, P. K. Studies on the Chemistry of $[Cd(NH_3)_4](MnO_4)_2$. A Low Temperature Synthesis Route of the $CdMn_2O_{4+x}$ Type NO_x and CH_3SH Sensor Precursor. *Z. Anorg. Allgem. Chem.* **2012**, *638*, 177−186.
(22) Kotai, L.; Banerji, K. K.; Sajo, I.; Kristof, J.; Sreedhar, B.; Holly, S.; Keresztury, G.; Rockenbauer, A. An Unprecedented-Type Intramolecular Redox Reaction of Solid Tetraamminecopper(2+) Bis(permanganate) ($[Cu(NH_3)_4](MnO_4)_2$) − A Low-Temperature Synthesis of Copper Dimanganese Tetraoxide-Type ($CuMn_2O_4$) Nanocrystalline Catalyst Precursors. *Helv. Chim. Acta* **2002**, *85*, 2316−2327.
(23) Morozov, I. V.; Lyubushkin, R. A.; Fedorova, A. A.; Petrov, M. N.; Burdeinaya, T. N.; Tret'yakov, V. F. Physicochemical Properties of Manganese-Containing Oxides with a Spinel Structure Prepared with the Use of Ammonium Nitrate and Their Catalytic Activity in Carbon Monoxide Oxidation. *Kinet. Catal.* **2006**, *47*, 35−39.
(24) Kótai, L.; Gács, I.; Kazinczy, B.; Sajó, I. E.; Sreedhar, B. Quasi-intramolecular acid-base reactions in aqueous solutions of metal complexes of basic ligands I. Generalized theoretical considerations

on the deammoniation of $[ML_n]X_n$ type ammonia complexes. *Transit. Metal Chem.* **2003**, *28*, 292−295.
(25) Kótai, L.; Horváth, T.; Szentmihályi, K.; Keszler, Ágnes. Evidence for quasi- intramolecular acid-base reactions in solutions of transition metal ammine complexes. *Transit. Metal Chem.* **2000**, *25*, 293−294.
(26) Kótai, L.; Szabó, P.; Keszler, Ágnes. Studies on the thermal behavior of ammonium permanganate. *Thermochim. Acta* **1999**, *338*, 129−133.
(27) Kótai, L.; Gács, I.; Sajó, I. E.; Sharma, P. K.; Banerji, K. K. Beliefs and facts in permanganate chemistry - an overview on the synthesis and reactivity of simple and complex permanganates. *Trends in Inorg. Chem.* **2009**, *11*, 25−104.
(28) Kovács, G. B.; May, N. V.; Bombicz, P. A.; Klébert, S.; Németh, P.; Menyhárd, A.; Novodárszki, G.; Petrusevski, V.; Franguelli, F. P.; Magyari, J.; Béres, K.; Szilágyi, I. M.; Kótai, L. *RSC Adv.* **2019**, *9*, 28387−28398.
(29) Gillot, B.; Buguet, S.; Kester, E. Oxidation mechanism and valence states of copper and manganese in tetragonal $CuMn_2O_4$. *J. Mater. Chem.* **1997**, *7*, 2513−2517.
(30) Lenglet, M.; Huysser, A. D.; Kasperek, J.; Bonnelle, J. P.; Durr, J. Characterization of the oxidation states of copper and manganese in some manganites by the analysis of the XPS spectrum, X emission, and X absorption thresholds. *Mater. Res. Bull.* **1985**, *20*, 745−757.
(31) Wagner, C. D.; Riggs, W. M.; Davis, L. E.; Moulder, J. F.; Muilenberg, G. E. *Handbook of X-Ray photoelectron spectroscopy*; Perkin Elmer Coorporation: Minnesota, 1979.
(32) Diodati, S.; Minelli, A.; Dolcet, P.; Gross, S. Transition Metal Manganites Prepared by a Green and Low-Temperature Wet Chemistry Route, Investigated by XPS. *Surf. Sci. Spectra* **2015**, *22*, 1−20.
(33) Hanke, W.; Ebel, H.; Ebel, M. F.; Jablonski, A.; Hirokawa, K. Quantitative XPS — multiline approach. *J. Electron Spectrosc. Relat. Phenom.* **1986**, *40*, 241−257.
(34) Mohai, M. Surface Investigation of Zinc Ferrite Nanopowders, In *XPS Multiquant: Application Example*; Research Centre of Natural Sciences, 2001.
(35) Mohai, M. XPS MultiQuant: multimodel XPS quantification software. *Surf. Interface Anal.* **2004**, *36*, 828−832.
(36) Sajó, I. E.; Bakos, L.; Szilagyi, I. M.; Lendvay, G.; Magyari, J.; Mohai, M.; Szegedi, Ágnes.; Farkas, A.; Jánosity, A.; Klébert, S.; Kótai, L. Unexpected Sequential NH_3/H_2O Solid/Gas Phase Ligand Exchange and Quasi-Intramolecular Self- Protonation Yield $[NH_4Cu(OH)MoO_4]$, a Photocatalyst Misidentified before as $(NH)_2Cu(MoO_4)_2$. *Inorg. Chem.* **2018**, *57*, 13679−13692.
(37) Fortunato, G.; Oswald, H.; Reller, A. Spinel-type oxide catalysts for low temperature CO oxidation generated by use of an ultrasonic aerosol pyrolysis process. *J. Mater. Chem.* **2001**, *11*, 905−911.
(38) Evans, S.; Pritchard, R. G.; Thomas, J. M. Relative differential subshell photoionisation cross-sections (MgK_α) from lithium to uranium. *J. Electron Spectrsc. Relat. Phenom.* **1978**, *14*, 341−358.
(39) Reilman, R. F.; Msezane, A.; Manson, S. T. Relative intensities in photoelectron spectroscopy of atoms and molecules. *J. Electron Spectrsc. Relat. Phenom.* **1976**, *8*, 389−394.

https://dx.doi.org/10.1021/acsomega.0c05301
ACS Omega 2021, 6, 1523−1533